

## COMPUTATIONAL STUDY OF DRUG DELIVERY SYSTEMS WITH RADIONUCLIDE AND FLUORESCENCE IMAGING MODALITIES. I. ALBUMIN-BASED SYSTEMS FOR DOXORUBICIN DELIVERY

 V. Trusova<sup>a\*</sup>,  U. Tarabara<sup>a</sup>, I. Karnaukhov<sup>b</sup>,  A. Zelinsky<sup>b</sup>,  B. Borts<sup>b</sup>, I. Ushakov<sup>b</sup>, L. Sidenko<sup>b</sup>,  G. Gorbenko<sup>a</sup>

<sup>a</sup>Department of Medical Physics and Biomedical Nanotechnologies, V.N. Karazin Kharkiv National University  
4 Svobody Sq., Kharkiv, 61022, Ukraine

<sup>b</sup>National Science Center "Kharkov Institute of Physics and Technology", Kharkiv, Ukraine

\*Corresponding Author: [valerija.trusova@karazin.ua](mailto:valerija.trusova@karazin.ua)

Received August 15, 2024, revised September 22, 2024; accepted November 3, 2024

Molecular docking and molecular dynamics methodologies were employed to design and evaluate delivery systems for the antineoplastic agent doxorubicin (DOX) utilizing human serum albumin (HSA) as the carrier. To engineer a drug delivery system (DDS) with dual imaging modalities, complexes of the radionuclide technetium-99m (TCC) and near-infrared (NIR) fluorescent dyes, including indocyanine green (IG), methylene blue (MB), heptamethine cyanine dye AK7-5, and squaraine dye SQ1, were integrated into the protein nanocarriers. The highest binding affinities to the proteins were identified for TCC [<sup>99m</sup>Tc]Tc-diisopropyl iminodiacetic acid (TcDIS), [<sup>99m</sup>Tc]Tc-hydrazinonicotinic acid-H6F (TcHYN), [<sup>99m</sup>Tc]Tc-Mebrofenin (TcMEB), as well as the fluorescent dyes IG and SQ1. Molecular docking analyses revealed that most technetium complexes (TCCs) bind to HSA domain I, with some exceptions showing affinity for domains I and III or domain III alone. Ternary and quaternary protein-ligand systems were explored using multiple ligand docking approaches. In ternary systems, DOX binding sites were identified either in domain I or in a region spanning multiple domains, depending on potential overlap with TCC binding sites. For quaternary systems incorporating NIR fluorophores, binding affinities decreased in the order: IG > SQ1 > AK7-5 > MB. Molecular dynamics simulations of HSA-DOX-MB and HSA-DOX-IG complexes demonstrated stable associations between the components, with consistent center-of-mass distances and minimal perturbation of HSA structure. These findings support the potential of HSA as a suitable carrier for developing dual-modality imaging nanocarriers incorporating both radionuclide and fluorescence imaging capabilities.

**Keywords:** Drug delivery systems; Human serum albumin; Doxorubicin; Technetium complexes; Fluorescent dyes; Molecular docking; Molecular dynamics

**PACS:** 87.14.C++c, 87.16.Dg

The development of targeted drug nanocarriers has emerged as a critical strategy in enhancing the therapeutic efficacy of anticancer agents while mitigating their systemic toxicity [1,2]. Among these, protein-based drug delivery systems (PDDS) have garnered significant attention due to their exceptional biocompatibility, biodegradability, and ability to accumulate in tumor tissues via the enhanced permeability and retention (EPR) effect [3,4]. Proteins offer unique advantages as drug delivery vehicles, including their natural abundance, renewable sources, and the presence of multiple functional groups for drug loading and targeting modifications. Albumin, a naturally occurring protein, has emerged as a promising carrier for drug delivery due to its biocompatibility, non-immunogenicity, and ability to bind and transport a wide range of therapeutic agents [5,6]. The use of albumin-based delivery systems offers several advantages, including prolonged circulation time, enhanced permeability and retention effect, and the potential for passive and active targeting of tumor tissues. In recent years, the integration of multimodal imaging modalities into drug delivery systems has gained significant attention [7,8]. Such systems not only facilitate the monitoring of drug distribution and accumulation in real-time but also provide valuable insights into the pharmacokinetics and pharmacodynamics of the therapeutic agents. In this study, we employed computational tools, specifically molecular docking and molecular dynamics simulations, to design albumin-based multimodal delivery systems for doxorubicin. Our approach involved the incorporation of radiopharmaceuticals, specifically technetium-99m (<sup>99m</sup>Tc) coordination complexes, and near-infrared (NIR) fluorescent dyes, including indocyanine green, methylene blue, heptamethine cyanine dye AK7-5, and squaraine dye SQ1. The integration of these imaging modalities aims to enhance the precision of drug delivery and enable the simultaneous tracking of therapeutic and diagnostic agents.

### METHODS

Human serum albumin (HSA) in its dimeric form (PDB ID: 1A06) was used as a main component of the designed PDDS. A therapeutic component of the examined drug delivery systems was represented by one of the most widespread antitumor drug doxorubicin (DOX), anthracycline antibiotic whose antineoplastic properties arise mainly from its abilities to intercalate into DNA, inhibit topoisomerase II, disrupt gene expression, generate reactive oxygen species and produce damage of cell membranes [9]. To design the PDDS, in the present study we used 12 <sup>99m</sup>Tc-based radiopharmaceuticals

(Fig. 1): [ $^{99m}\text{Tc}$ ]Tc-Sestamibi (TcSES), [ $^{99m}\text{Tc}$ ]Tc-Tetrofosmin (TcTET), [ $^{99m}\text{Tc}$ ]Tc-Medronate (TcMED), [ $^{99m}\text{Tc}$ ]Tc-dimercaptosuccinic acid (TcDMSA), [ $^{99m}\text{Tc}$ ]Tc-diethylenetriaminepentaacetate (Tc-DTPA), [ $^{99m}\text{Tc}$ ]Tc-mercaptoacetyltriglycine (TcMAG), Pertechnetate [ $^{99m}\text{Tc}$ ]TcO $_4^-$  (TcPER), [ $^{99m}\text{Tc}$ ]Tc-Exametazime (TcEXA), [ $^{99m}\text{Tc}$ ]Tc-diisopropyl iminodiacetic acid (TcDIS), [ $^{99m}\text{Tc}$ ]Tc-ethylene cysteine dimer (TcECD), [ $^{99m}\text{Tc}$ ]Tc- hydrazinonicotinic acid-H6F (TcHYN), [ $^{99m}\text{Tc}$ ]Tc-Mebrofenin (TcMEB). To create the dual-labelled PDDS with both nuclear and optical imaging modalities, the examined protein systems were loaded by the binary combinations of the above  $^{99m}\text{Tc}$  complexes and four NIR fluorescent dyes (FD), Methylene Blue (MB), Indocyanine Green (IG), cyanine AK7-5 and squaraine SQ1 (Fig. 2). To identify the most energetically favorable binding sites for TCC, DOX, FD in the HSA, HSA-Lz, HSA-TRF, HSA-Hb protein systems the molecular docking studies were performed using the HDock server.60 Prior to the docking procedure, the structures of HSA dimers and its complexes with Lz, TRF and Hb were relaxed through 1 ns MD simulations. The structures of ligands were built in MarvinSketch (version 18.10.0) and the geometries were further optimized in Avogadro (version 1.1.0). The selected docking poses were visualized with the UCSF Chimera software (version 1.14) and analyzed with Protein-Ligand Interaction Profiler [10]. The molecular dynamics simulations were performed to evaluate the stability of some of the examined protein-ligand assemblies, viz. the ternary complexes HSA – DOX – IG and HSA – DOX – MB. The input files for MD calculations were prepared using the CHARMM-GUI input generator [11]. The .itp files of DOX, IG and MB were obtained from the corresponding .mol2 files, using the CHARMM General Force Field, followed by the correction of the dye/drug partial charges according to those assigned by RESP ESP charge Derive Server [12]. The drug-dye-protein complexes were solvated in a rectangular box with a minimum distance of 10 Å from the protein to the box edges and 0.15 M NaCl (neutralizing ions) were added to the systems. The TIP3P water model was used. The molecular dynamics simulations and analysis of the trajectories were performed using the GROMACS software (version 2023.3) with the CHARMM36m force field in the NPT ensemble with the time step for MD simulations 2 fs. The calculations were performed at a temperature of 310 K using the V-rescale thermostat. The minimization and equilibration of the systems were carried out during 50000 and 125000 steps, respectively. The time interval for MD calculations was 1 ns HSA – DOX – MB complex and 10 ns for HSA – DOX – IG complex. The correction of MD trajectories after the MD run, was performed using the `gmx trjconv` GROMACS command. The visualization of the snapshots of MD runs and calculations of the protein backbone root-mean-square deviation (RMSD), the protein solvent-accessible surface area (SASA), and the distances between the centers of mass of protein and ligand were performed in VMD.

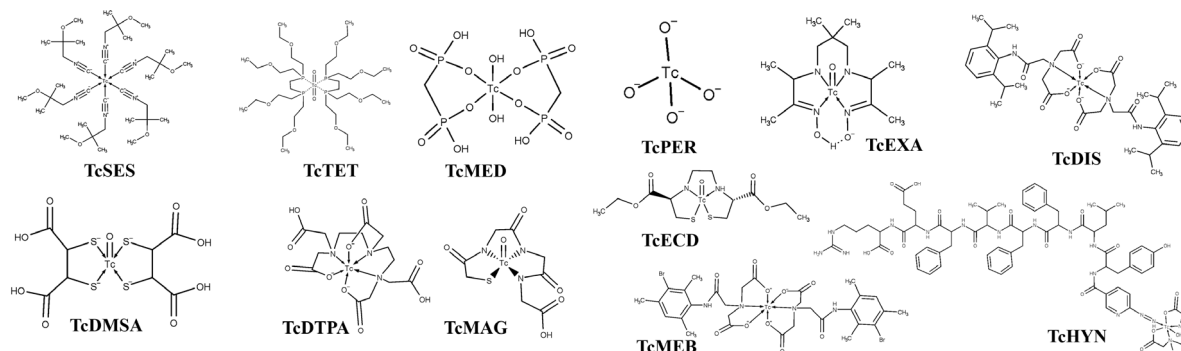


Figure 1. Chemical structures of Technetium-99m complexes

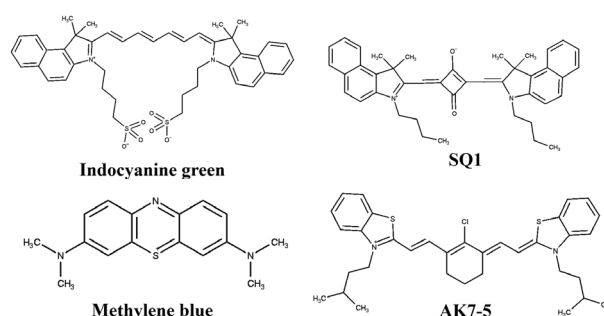


Figure 2. Chemical structures of fluorescent dyes

## RESULTS AND DISCUSSION

At the first step of the study, we compared the binding affinities of different  $^{99m}\text{Tc}$  pharmaceuticals for HSA. Shown in Fig. 3 are the best score complexes of TCC with the albumin dimer. A polypeptide chain of HSA monomer contains 585 amino acid residues with three homologous domains: I (amino acid residues 1-195), II (amino acid residues 196-383), and III (amino acid residues 384-585). Each of these three domains consists of two subdomains (A and B), stabilized by 17 disulfide bonds. It is generally recognized that the majority of drugs bind to HSA through the two sites known as

Sudlow sites I and II, which are located in hydrophobic cavities of subdomains IIA and IIIA, respectively [13]. It appeared that the binding sites for the five TCC (TcMED, TcEXA, TcECD, TcDMSA, TcDTPA) are situated on the domain I, within the region extending from LEU115 to LYS190 and all contain 7 identical amino acid residues LEU115, ARG117, TYR138, ILE142, TYR161, LEU182 and ARG186 (Fig. 3., Table 1). The consistency in binding location suggests a common structural recognition mechanism for these TCCs by HSA, which may be attributed to the physicochemical properties shared among these compounds. This finding is particularly relevant as it indicates a potential competitive binding scenario among these TCCs, which could influence their pharmacokinetics when administered concurrently or in close succession.

A high degree of similarity is observed also for TcTET and TcDIS, which both form contacts with the residues of the domains I and III (ASN<sub>109</sub>, ARG<sub>114</sub>, LEU<sub>115</sub>, ARG<sub>145</sub>, LYS<sub>190</sub>, GLU<sub>425</sub>, GLU<sub>520</sub>, ILE<sub>523</sub>). Likewise, the complexes of TcSES and TcMEB with HSA share similar amino acid residues GLU<sub>188</sub>, LYS<sub>195</sub>, ARG<sub>218</sub>, ARG<sub>222</sub>, GLU<sub>292</sub>, VAL<sub>293</sub>, HSD<sub>440</sub> and TYR<sub>452</sub>. This divergent binding pattern implies a potentially different mode of interaction for these TCCs with HSA. The distinct binding site for TcSES and TcMEB suggests that these compounds may not directly compete with the majority of TCCs for HSA binding, potentially allowing for their use in combination with other <sup>99m</sup>Tc pharmaceuticals without significant pharmacokinetic interference. The binding site for TcPER is located in the domain I, while the interface residues of the complex HSA-TcMAG encompass all protein domains.

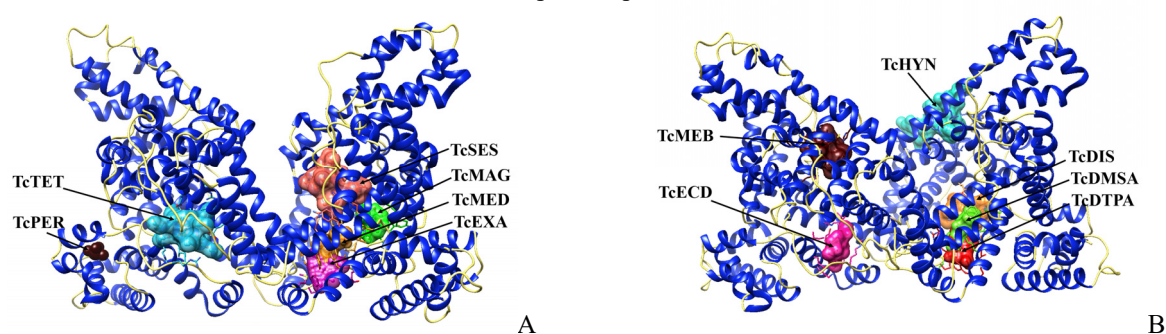


**Figure 3.** The most energetically favorable complexes of TCC with HSA

**Table 1.** The interface amino acid residues and the types of interactions involved in the binding of technetium 99m complexes (TCC) to human serum albumin (HSA)

TCC	HSA-TCC interface residues	Types of interactions
TcSES	TYR <sub>150A</sub> *, GLU <sub>153A</sub> , PHE <sub>156A</sub> , PHE <sub>157A</sub> , ARG <sub>160A</sub> , GLU <sub>188A</sub> , ALA <sub>191A</sub> , SER <sub>192A</sub> , LYS <sub>195A</sub> , GLN <sub>196A</sub> , LYS <sub>199A</sub> , ARG <sub>218A</sub> , ARG <sub>222A</sub> , HSD <sub>288A</sub> , GLU <sub>292A</sub> , VAL <sub>293A</sub> , LYS <sub>436A</sub> , HSD <sub>440A</sub> , TYR <sub>452A</sub>	Hydrophobic interactions, hydrogen bonds
TcTET	ASN <sub>109B</sub> , ARG <sub>114B</sub> , LEU <sub>115B</sub> , ARG <sub>145B</sub> , LYS <sub>190B</sub> , GLU <sub>425B</sub> , ARG <sub>428B</sub> , GLU <sub>520B</sub> , ILE <sub>523B</sub>	Hydrophobic interactions, hydrogen bonds
TcMED	LEU <sub>115A</sub> , ARG <sub>117A</sub> , TYR <sub>138A</sub> , ILE <sub>142A</sub> , HSD <sub>146A</sub> , PHE <sub>149A</sub> , LEU <sub>154A</sub> , PHE <sub>157A</sub> , TYR <sub>161A</sub> , LEU <sub>182A</sub> , ASP <sub>183A</sub> , LEU <sub>185A</sub> , ARG <sub>186A</sub> , ASP <sub>187A</sub> , GLY <sub>189A</sub> , LYS <sub>190A</sub>	Hydrogen bonds
TcMAG	ASP <sub>107A</sub> , ASP <sub>108A</sub> , ASN <sub>109A</sub> , ARG <sub>145A</sub> , HSD <sub>146A</sub> , PRO <sub>147A</sub> , TYR <sub>148A</sub> , LYS <sub>190A</sub> , ALA <sub>191A</sub> , SER <sub>193A</sub> , ALA <sub>194A</sub> , ARG <sub>197A</sub> , GLU <sub>425A</sub> , ASN <sub>458A</sub> , GLN <sub>459A</sub>	Hydrogen bonds, salt bridges
TcEXA	LEU <sub>115A</sub> , VAL <sub>116A</sub> , ARG <sub>117A</sub> , PRO <sub>118A</sub> , MET <sub>123A</sub> , PHE <sub>134A</sub> , LYS <sub>137A</sub> , TYR <sub>138A</sub> , LEU <sub>139A</sub> , GLU <sub>141A</sub> , ILE <sub>142A</sub> , ARG <sub>145A</sub> , TYR <sub>161A</sub> , PHE <sub>165A</sub> , LEU <sub>182A</sub> , ARG <sub>186A</sub>	Hydrophobic interactions, hydrogen bonds
TcECD	LEU <sub>115B</sub> , ARG <sub>117B</sub> , PRO <sub>118B</sub> , MET <sub>123B</sub> , PHE <sub>134B</sub> , LYS <sub>137B</sub> , TYR <sub>138B</sub> , GLU <sub>141B</sub> , ILE <sub>142B</sub> , TYR <sub>161B</sub> , LEU <sub>182B</sub> , ASP <sub>183B</sub> , LEU <sub>185B</sub> , ARG <sub>186B</sub>	Hydrophobic interactions, hydrogen bonds, salt bridges
TcDMSA	LEU <sub>115A</sub> , VAL <sub>116A</sub> , ARG <sub>117A</sub> , PRO <sub>118A</sub> , MET <sub>123A</sub> , TYR <sub>138A</sub> , ILE <sub>142A</sub> , HSD <sub>146A</sub> , PHE <sub>149A</sub> , LEU <sub>154A</sub> , PHE <sub>157A</sub> , TYR <sub>161A</sub> , LEU <sub>182A</sub> , LEU <sub>185A</sub> , ARG <sub>186A</sub> , ASP <sub>187A</sub> , GLU <sub>188A</sub> , GLY <sub>189A</sub> , LYS <sub>190A</sub>	Hydrogen bonds, salt bridges
TcDIS	ASN <sub>109A</sub> , PRO <sub>110A</sub> , LEU <sub>112A</sub> , ARG <sub>114A</sub> , LEU <sub>115A</sub> , ARG <sub>145A</sub> , HSD <sub>146A</sub> , ARG <sub>186A</sub> , LYS <sub>190A</sub> , PRO <sub>421A</sub> , GLU <sub>425A</sub> , GLU <sub>520A</sub> , ILE <sub>523A</sub>	Hydrophobic interactions, hydrogen bonds
TcPER	TYR <sub>30B</sub> , HSD <sub>67B</sub> , THR <sub>68B</sub> , PHE <sub>70B</sub> , GLY <sub>71B</sub> , LEU <sub>74B</sub> , GLU <sub>95B</sub> , ARG <sub>98B</sub> , ASN <sub>99B</sub> , PHE <sub>102B</sub>	Hydrogen bonds
TcDTPA	LEU <sub>115A</sub> , VAL <sub>116A</sub> , ARG <sub>117A</sub> , PRO <sub>118A</sub> , MET <sub>123A</sub> , PHE <sub>134A</sub> , LEU <sub>135A</sub> , LYS <sub>137A</sub> , TYR <sub>138A</sub> , GLU <sub>141A</sub> , ILE <sub>142A</sub> , TYR <sub>161A</sub> , LEU <sub>182A</sub> , ARG <sub>186A</sub>	Hydrogen bonds, salt bridges
TcHYN	GLU <sub>383A</sub> , LEU <sub>387A</sub> , ASN <sub>391A</sub> , LEU <sub>394A</sub> , LEU <sub>407A</sub> , VAL <sub>409A</sub> , ARG <sub>410A</sub> , TYR <sub>411A</sub> , LEU <sub>430A</sub> , LEU <sub>453A</sub> , GLU <sub>492A</sub> , SER <sub>489A</sub> , LYS <sub>541A</sub> , GLU <sub>542A</sub> , LYS <sub>545A</sub>	Hydrogen bonds, $\pi$ -stacking, salt bridges
TcMEB	GLU <sub>188B</sub> , LYS <sub>195B</sub> , TRP <sub>214B</sub> , ARG <sub>218B</sub> , GLN <sub>221B</sub> , ARG <sub>222B</sub> , GLU <sub>292B</sub> , VAL <sub>293B</sub> , GLU <sub>294B</sub> , ASN <sub>295B</sub> , LYS <sub>436B</sub> , HSD <sub>440B</sub> , LYS <sub>444B</sub> , PRO <sub>447B</sub> , CYS <sub>448B</sub> , ALA <sub>449B</sub> , ASP <sub>451B</sub> , TYR <sub>452B</sub>	Hydrophobic interactions, hydrogen bonds, salt bridges

Meanwhile, TcHYN, which in contrast to the other TCC, possesses a specific peptide (YLFFVFER) in its structure (Fig. 1), binds to HSA on the domain III, with some of the interface residues (ARG<sub>410</sub>, TYR<sub>411</sub>, SER<sub>489</sub>) belonging to

the Sudlow site II. Furthermore, as judged from the comparison of the best docking scores (BDS) for the HSA-TCC complexes (Fig. 4), TcHYN has the highest affinity for HSA, with BDS values following the order TcHYN > TcDTPA > TcDIS > TcMEB > TcDMSA > TcSES > TcTET > TcMED > TcMAG > TcECD > TcEXA > TcPER. The highest affinity of TcHYN for HSA suggests that peptide conjugation could be a promising strategy for enhancing the albumin-binding properties of radiopharmaceuticals, potentially leading to improved in vivo stability and target tissue accumulation.

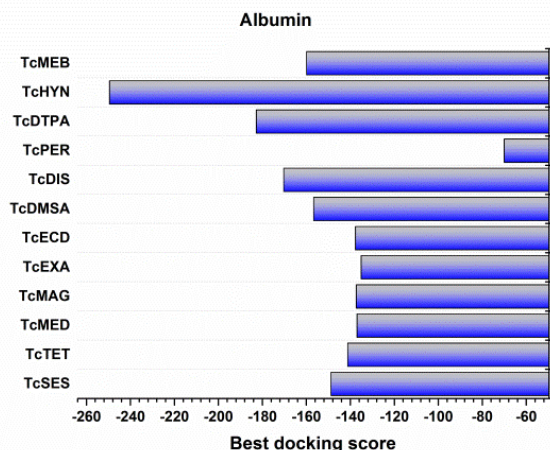


**Figure 4.** The best docking score values obtained for the TCC complexes with HSA

At the next steps of the investigation, we employed the multiple ligand docking approach [14] to explore the ternary (HSA-TCC-DOX) and quaternary (HSA-TCC-DOX-FD) protein-ligand systems. The ternary systems were obtained by the docking of doxorubicin to the best score complexes of TCC with HSA (Fig. 5). The following features of the ternary systems are worthy of mention: i) when the HSA binding sites for TCC and DOX do not overlap, the DOX binding site is located in the domain I of HSA molecule, encompassing 16 residues from the region flanked with PRO<sub>113</sub> and ARG<sub>186</sub> (site HSA<sub>113-186</sub>) (Fig. 5, A); ii) when the HSA binding sites for TCC and DOX overlap with each other (as in the cases of TcMED, TcEXA, TcDMSA and TcDTPA), DOX binds to another HSA site containing 23 amino acid residues from the region flanked with ASP<sub>107</sub> and GLN<sub>459</sub> (Fig. 5, B).

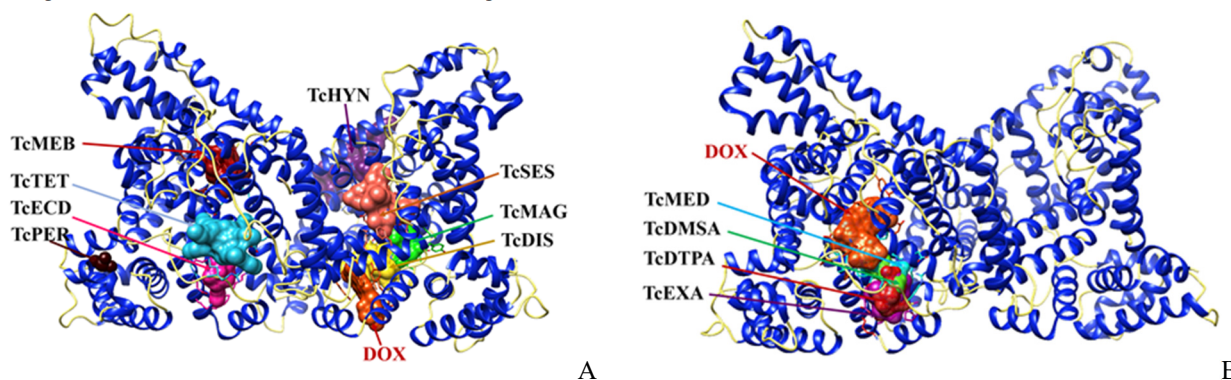


**Figure 5.** The highest affinity binding sites for DOX in the HSA-TCC systems

Next, to obtain the systems with dual imaging modality, the best score complexes HSA-TCC-DOX were docked with one of four NIR fluorophores, two traditionally used dyes, methylene blue and indocyanine green, and two emerging fluorophores, heptamethine cyanine dye AK7-5, and squaraine dye SQ1. A comparative analysis of the docking results obtained for the quaternary systems (HSA + TCC + DOX + FD) indicates that the affinities of the examined dyes for HSA/HSA-DOX decrease in the row: IG (BDS = -207.2/-190.3) > SQ1 (BDS = -186.1/-185.9) > AK7-5 (BDS = -162.4/-162.9) > MB (BDS = -127.1/-117.3). This hierarchy of binding affinities provides crucial information for the selection of optimal fluorophores in the context of technetium-based dual-modality imaging systems. While the amino acid composition of the fluorophore binding sites varied across different technetium complexes and protein components, a consistent pattern emerged, allowing for the identification of predominant interaction sites for each system. Notably, a specific albumin site, designated as HSA<sub>115-186</sub>, was identified as the preferential binding region for MB in both HSA-DOX and HSA-TCC-DOX complexes (Fig. 6). This finding suggests a potential interaction between the technetium complexes and the fluorophores, which could have implications for the overall stability and efficacy of the dual-modality imaging system.

At the last step of the study, we performed the molecular dynamics simulation of two of the examined complexes, to assess their stability in aqueous solution. Because of the problems associated with the parametrization of <sup>99m</sup>Tc complexes the MD simulations were carried out for the systems HSA-DOX-MB and HSA-DOX-IG. As illustrated in Fig. 7, DOX and FD remain bound to HSA during the simulation time (1 ns for MB and 10 ns for IG).

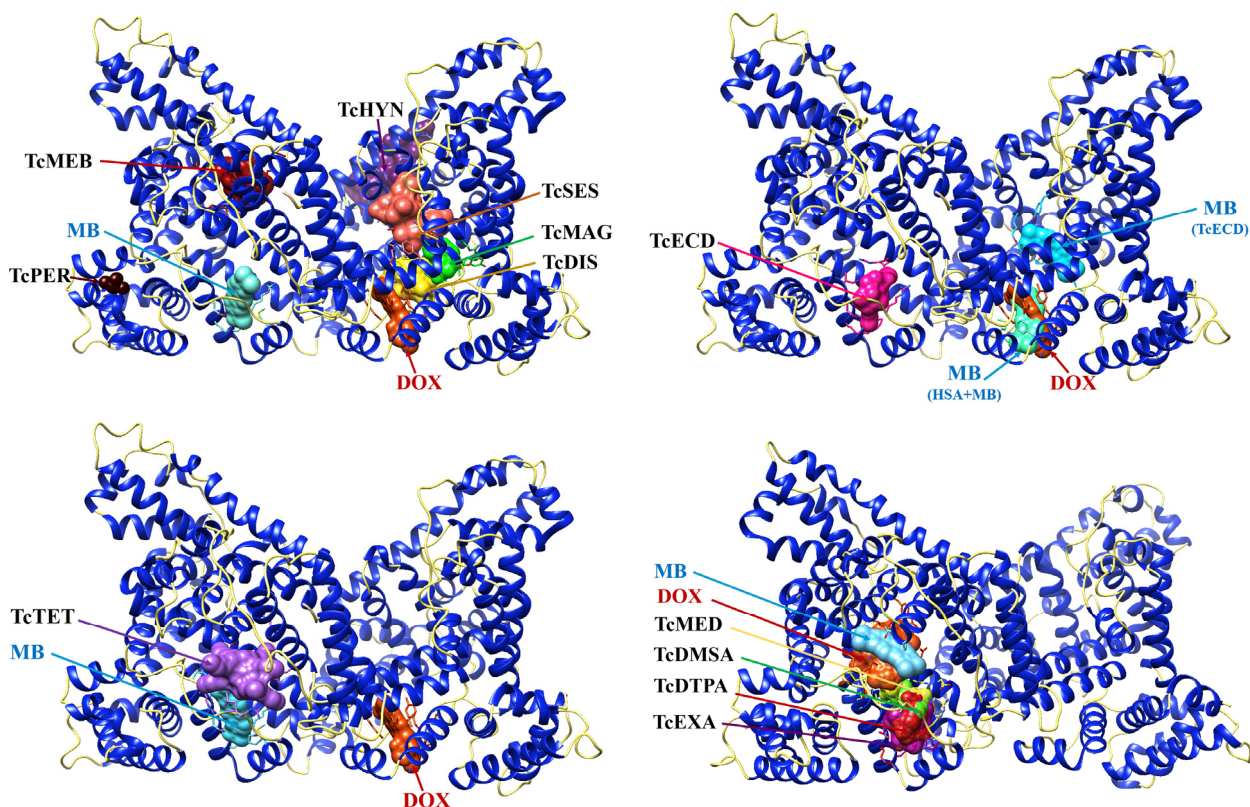


**Figure 6.** The most energetically favorable docking poses in the complexes with HSA-TCC-DOX-MB

The persistence of DOX and fluorescent dye (FD) binding to HSA throughout the simulation periods (1 ns for MB and 10 ns for IG) suggests a stable association between these components. This stability is further corroborated by the relatively consistent center-of-mass distances observed between the protein and ligands. The IG system exhibited distances ranging from 2.4 to 2.8 nm, while the MB system showed distances between 2.3 and 2.7 nm. DOX maintained the closest proximity to HSA, with distances varying from 2.2 to 2.5 nm. These findings indicate that all ligands remain in close association with HSA, with DOX potentially exhibiting the strongest interaction (Fig. 8, A, B).

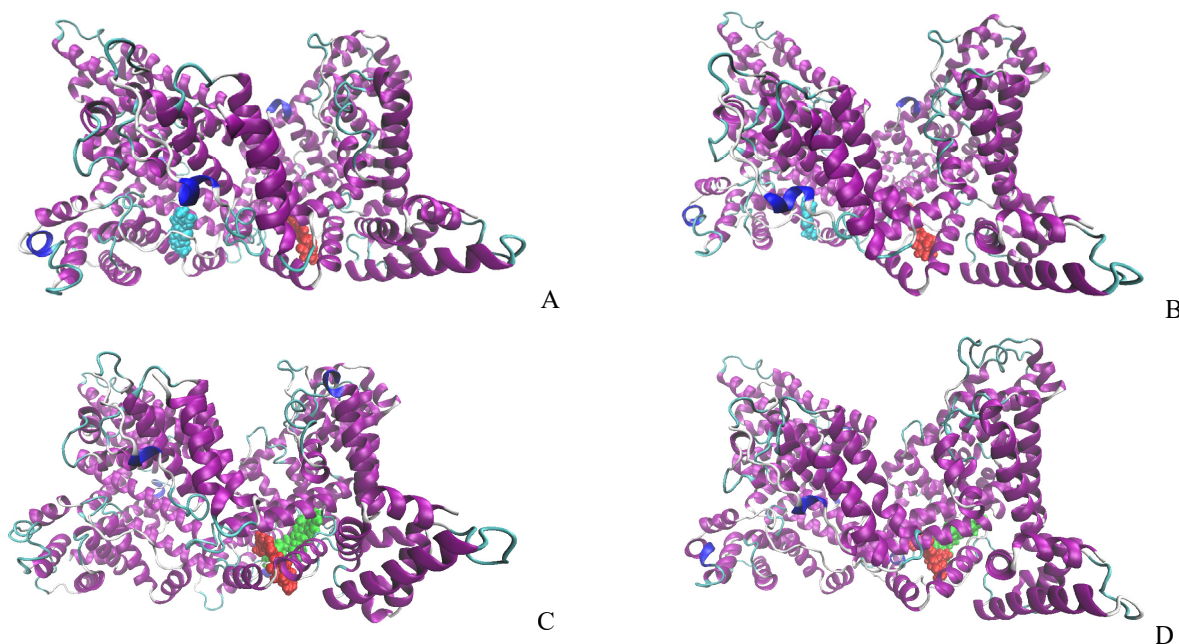


**Figure 7.** The snapshots of HSA-DOX-MB (A, B) and HSA-DOX-IG (C, D) complexes corresponding to the timepoints of 0 ns (A, C); 1 ns (B) and 10 ns (D).

The structural integrity of the HSA molecule in the presence of DOX, MB, and IG was assessed through Root Mean Square Deviation (RMSD) and Solvent Accessible Surface Area (SASA) analyses. The results suggest that the albumin

structure remains largely unperturbed upon ligand binding, as evidenced by the absence of significant fluctuations in these parameters (Fig. 8, C-F). This structural stability is crucial for maintaining the functional properties of HSA as a drug carrier.

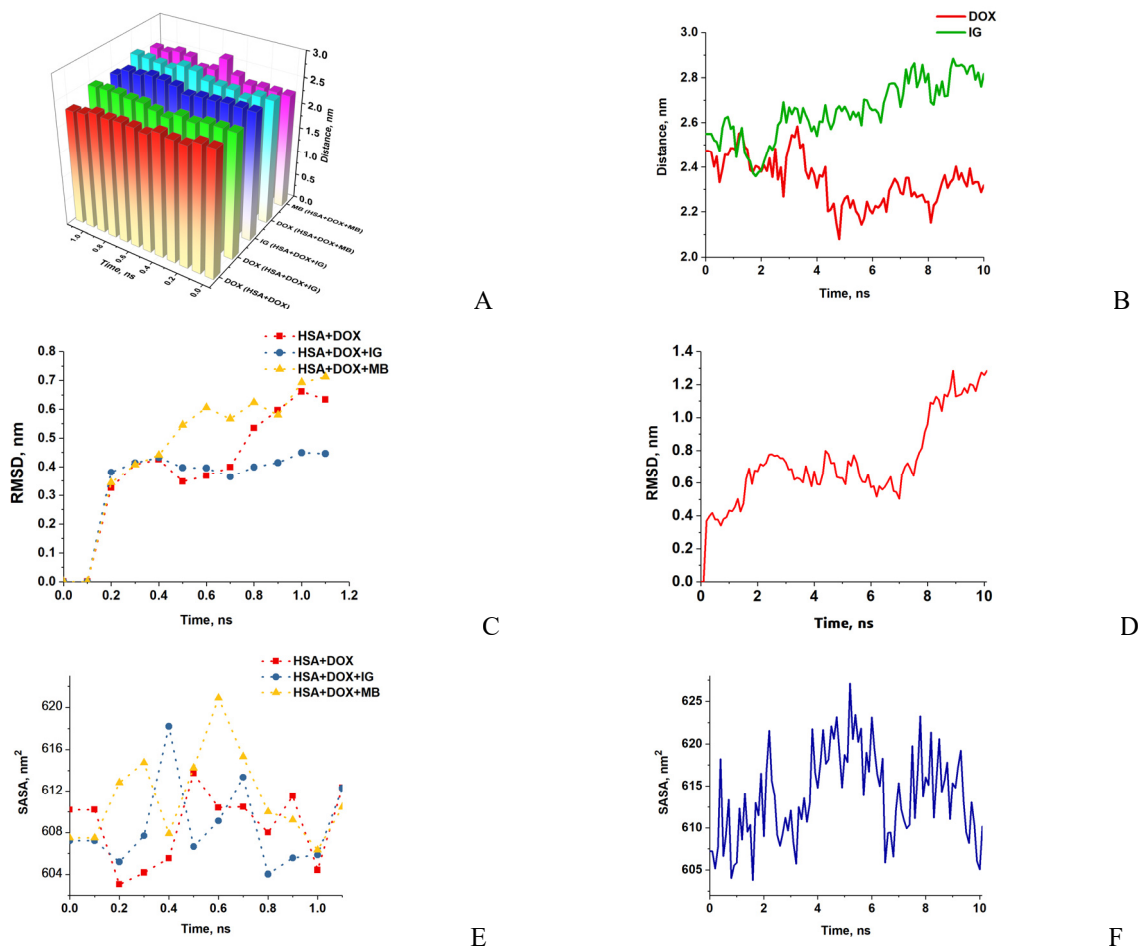


**Figure 8.** The distances between the centers of mass (A, B), RMSD (root mean square deviation) of the protein backbone atoms (C, D) and SASA (solvent accessible surface area) (E, F) calculated for the systems HSA-DOX, HSA-DOX-MB and HSA-DOX-IG.

Taken together, our findings indicate that HSA is suitable for the development of the DOX nanocarriers with both radionuclide and fluorescence imaging modalities.

## CONCLUSIONS

The collective findings from this study provide strong evidence supporting the suitability of HSA as potential platform for developing DOX nanocarriers with dual imaging modalities. The demonstrated stability of these complexes, coupled with their ability to incorporate both radionuclide and fluorescence imaging agents, presents a promising avenue for advancing targeted drug delivery systems with enhanced diagnostic capabilities. It is important to note, however, that while these results are encouraging, further studies are warranted to fully elucidate the long-term stability, pharmacokinetics, and in vivo efficacy of these systems. Additionally, the impact of technetium complexes on the overall stability and functionality of these nanocarriers remains to be explored, necessitating the development of more accurate parametrization methods for  $^{99m}\text{Tc}$  in future MD simulations.

## Acknowledgements

This project has received funding through the EURIZON project, which is funded by the European Union under grant agreement No.871072.

## ORCID

© Valeriya Trusova, <https://orcid.org/0000-0002-7087-071X>; © Uliana Tarabara, <https://orcid.org/0000-0002-7677-0779>  
© Galyna Gorbenko, <https://orcid.org/0000-0002-0954-5053>; © Andrey Zelinsky, <https://orcid.org/0000-0002-4110-8523>  
© Borys Borts, <https://orcid.org/0000-0002-1492-4066>

## REFERENCES

- [1] S. Adepu, S. Ramakrishna, *Molecules*. **26**, 5905 (2021). <https://doi.org/10.3390/molecules26195905>
- [2] Y. Sung, S. Kim, *Biomater. Res.* **24**, 12 (2020). <https://doi.org/10.1186/s40824-020-00190-7>

- [3] D. Jao, Y. Xue, J. Medina, X. Hu, *Materials (Basel)*. **10**, 517 (2017). <https://doi.org/10.3390/ma10050517>
- [4] S. Hong, D. Choi, H. Kim, C. Park, W. Lee, H. Park, *Pharmaceutics*. **12**, 604 (2020). <https://doi.org/10.3390/pharmaceutics12070604>
- [5] M. Larsen, M. Kuhlmann, M. Hvam, K. Howard, *Mol. Cell Ther.* **4**, 3 (2016). <https://doi.org/10.1186/s40591-016-0048-8>
- [6] A. Spada, J. Emami, J. Tuszynski, A. Lavasanifar, *Mol. Pharmaceutics*. **18**, 1862-1894 (2021). <https://doi.org/10.1021/acs.molpharmaceut.1c00046>
- [7] S. Hari, A. Gauba, N. Shrivastava, R. Tripathi, S. Jain, A. Pandey, *Drug Deliv. Transl. Res.* **13**, 135-163 (2023). <https://doi.org/10.1007/s13346-022-01197-4>
- [8] Q. Shubhra, K. Guo, Y. Liu, M. Razzak, M. Serajum, A. Moshui, *Acta Biomater.* **131**, 493-507 (2021). <https://doi.org/10.1016/j.actbio.2021.06.016>
- [9] M. Kciuk, A. Gielecinska, S. Mujwar, D. Kołat, Z. Kałuzinska-Kołat, I. Celik, R. Kontek, *Cells*. **12**, 659 (2023). <https://doi.org/10.3390/cells12040659>
- [10] M. F. Adasme, K. L. Linnemann, S. N. Bolz, F. Kaiser, S. Salentin, V. J. Haupt, M. Schroeder, *Nucl. Acids Res.* **49**, W530-W534 (2021). <https://doi.org/10.1093/nar/gkab294>
- [11] J. Lee, X. Cheng, J. M. Swails, M. S. Yeom, P. K. Eastman, J. A. Lemkul, S. Wei, J. Buckner, J. C. Jeong, Y. Qi, S. Jo, V. S. Pande, D. A. Case, C. L. Brooks, III, A. D. MacKerell, Jr., J. B. Klauda, W. Im, *Chem. Theory Comput.* **12**, 405-413 (2016). <https://doi.org/10.1021/acs.jctc.5b00935>
- [12] E. Vanquelef, S. Simon, G. Marquant, E. Garcia, G. Klimerak, J.C. Delepine, P. Cieplak, F.Y. Dupradeau, *Nucleic Acids Res.* **39**, W511-W517 (2011). <https://doi.org/10.1093/nar/gkr288>
- [13] S. Patel, K. K. Sharma and A. Datta, *Spectrochim. Acta A Mol. Biomol. Spectrosc.* **138**, 925-931 (2015). <https://doi.org/10.1016/j.saa.2014.10.015>
- [14] H. Li, C. Li, *Comput. Chem.* **31**, 2014-2022 (2010). <https://doi.org/10.1002/jcc.21486>

**КОМП'ЮТЕРНЕ ДОСЛІДЖЕННЯ СИСТЕМ ДОСТАВКИ ЛІКІВ З РАДІОНУКЛІДНИМИ  
ТА ФЛУОРЕСЦЕНТНИМИ МОДАЛЬНОСТЯМИ ВІЗУАЛІЗАЦІЇ. І. СИСТЕМИ НА ОСНОВІ АЛЬБУМІНУ  
ДЛЯ ДОСТАВКИ ДОКСОРУБІЦИНУ**

**В. Трусова<sup>a</sup>, У. Тарабара<sup>a</sup>, І. Карнаухов<sup>b</sup>, А. Зелінський<sup>b</sup>, Б. Борц<sup>b</sup>, І. Ушаков<sup>b</sup>, Л. Сіденко<sup>b</sup>, Г. Горбенко<sup>a</sup>**

<sup>a</sup>*Кафедра медичної фізики та біомедичних нанотехнологій, Харківський національний університет імені В.Н. Каразіна  
м. Свободи 4, Харків, 61022, Україна*

<sup>b</sup>*Національний науковий центр «Харківський фізико - технічний інститут», Харків, вул. Академічна, 1, 61108, Україна*

Методи молекулярного докінгу та молекулярної динаміки були використані для дизайну та оцінки стабільності систем доставки антинеопластичного агента доксорубіцину (ДОКС) з використанням людського сироваткового альбуміну (ЛСА) як наноносія. Для створення системи доставки ліків (СДЛ) з компонентами дуальної візуалізації, комплекси радіонукліду технецію-99m (ТСС) та ближньоінфрачервоних (БЧ) флуоресцентних барвників, включаючи індоціаніновий зелений (ІЗ), метиленовий синій (МС), гептаметиновий ціаніновий барвник АК7-5 та сквараїновий барвник SQ1, були інтегровані в білкові наноносії. Найвищі спорідненості до білків були виявлені для ТСС [<sup>99m</sup>Tc]Tc-діізопропіл імінооцтової кислоти (TcDIS), [<sup>99m</sup>Tc]Tc-гідразинонікотинової кислоти-Н6F (TcHYN), [<sup>99m</sup>Tc]Tc-Мebroфеніну (TcMEB), а також для флуоресцентних барвників ІЗ та SQ1. Результати молекулярного докінгу показали, що більшість комплексів технецію зв'язуються з доменом І ЛСА, за деякими винятками, що показують спорідненість до доменів І та ІІІ або лише до домену ІІІ. Три- та чотирикомпонентні системи білок-ліганд були досліджені за допомогою методології множинного докінгу лігандів. У трикомпонентних системах місця зв'язування ДОКС були ідентифіковані або в домені І, або в області, що охоплює кілька доменів, залежно від потенційного перекриття з місцями зв'язування ТСС. Для чотирикомпонентних систем, що включають БЧ флуорофори, спорідненість зв'язування зменшувалася в порядку: ІЗ > SQ1 > АК7-5 > МС. Аналіз профілів молекулярної динаміки комплексів БСА-ДОКС-МС та БСА-ДОКС-ІЗ продемонстрував стабільність досліджуваних комплексів з незмінними відстанями до центру мас та незначними порушеннями структури БСА. Отримані результати свідчать про потенціал БСА як наноносія лікарських засобів з модальністю дуальної візуалізації на основі радіонукліду та флуоресцентного барвника.

**Ключові слова:** системи доставки ліків; людський сироватковий альбумін; доксорубіцин; комплекси технецію; флуоресцентні барвники; молекулярний докінг; молекулярна динаміка